FIGURES

Figure 1 *– Model overview of hepatic galactose metabolism on cellular, tissue- and organ-scale and application in prediction of individual galactose clearance*

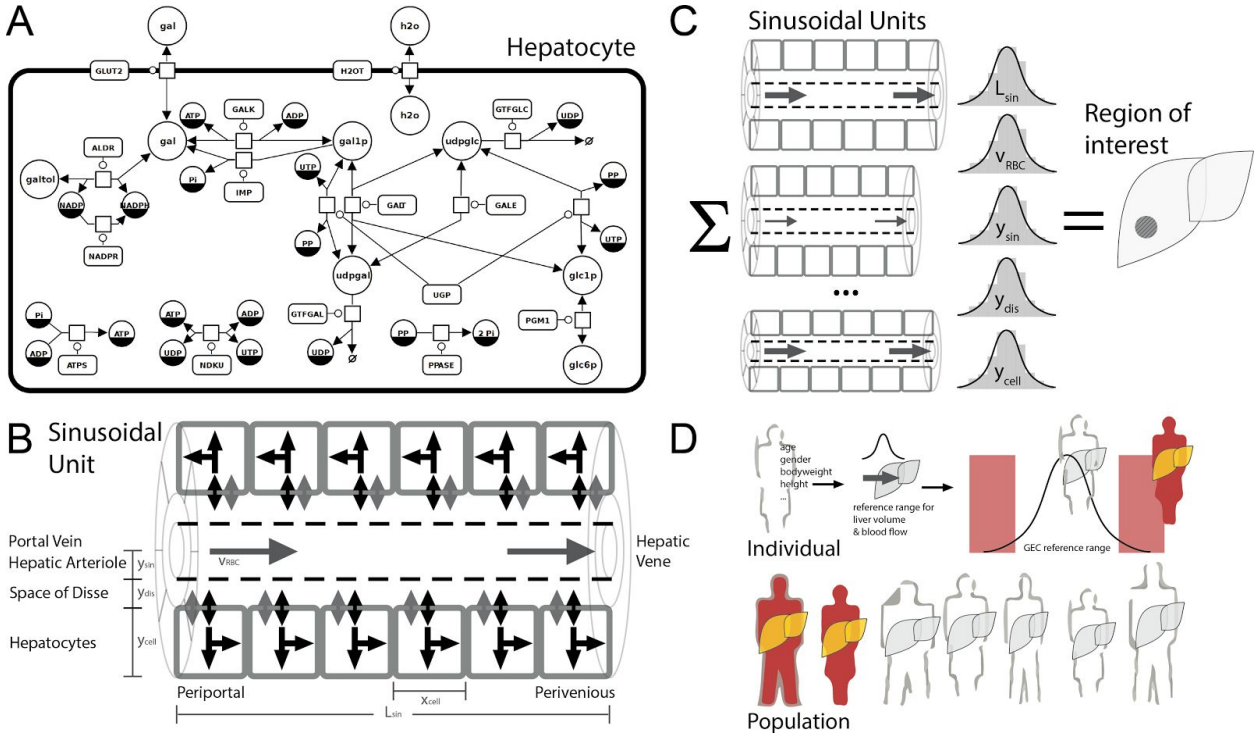

A) Overview of detailed kinetic model of hepatic galactose metabolism in SBGN {LeNovere2009}.
Reactions: (ALDR) **Aldose reductase (galactitol NAD 1-oxidoreductase);** (ATPS) **ATP synthesis;** (GALDH) **Galactose 1-dehydrogenase;** (GALE) **UDP-glucose 4-epimerase;** (GALK) **Galactokinase;** (GALT) **Galactose-1-phosphate uridyl transferase;** (GLUT2) **Facilitated glucose transporter member 2;** (GTFGAL) **Glycosyltransferase galactose;** (GTFGLC) **Glycosyltransferase glucose;** (NADPR) **NADP reductase;** (NDKU) **Nucleoside diphosphokinase, ATP:UDP phosphotransferase;** (IMP) **Inositol monophosphatase;** (PGM1) **Phosphoglucomutase-1;** (PPASE) **Pyrophosphatase;** (UGALP) **UDP-galactose pyrophosphorylase;** (UGP) **UDP-glucose pyrophosphorylase;**
Metabolites: (adp) **ADP;** (atp) **ATP;** (gal) **D-galactose;** (gal1p) **D-galactose 1-phosphate;** (galnat) **D-galactonate;** (galtol) **D-galactitol;** (glc) **D-glucose;** (glc1p) **D-glucose 1-phosphate;** (glc6p) **D-glucose 6-phosphate;** (nadp) **NADP;** (nadph) **NADPH;** (pi) **phosphate;** (pp) **pyrophosphate;** (udp) **UDP;** (udpgal) **UDP-D-galactose;** (udpglc) **UDP-D-glucose;** (utp) **UTP;**
B) Tissue-scale model of the sinusoidal unit comprising diffusion and convection based transport of substances in the sinusoid, diffusion-based transport of substances in the space of Disse and description of cellular metabolism via kinetic models of individual hepatocytes. Blood coming from the hepatic artery and portal vein enters the sinusoidal unit periportal and leaves pericentral. Transport between the sinusoid and the space of Disse occurs via fenestrations in the endothelial cells. Parameters and references are provided in the supplement.
C) Region of interests of the liver are modeled via the integration of multiple sinusoidal units based on the observed heterogeneity of structural parameters and microcirculation within the lobulus.

D) Based on anthropomorphic information of subjects like age, gender, bodyweight and height the region of interests are scaled to the observed distributions of liver blood flow and liver volume. Reference values of galactose clearance (GEC) are calculated and the experimental value of GEC can be evaluated in this reference context. Based on available data on the distribution of anthropomorphic features (NHANES {REF}) the population variability can be evaluated.

Figure 2 *– Parameter distributions and resulting multiple-indicator dilution curves*

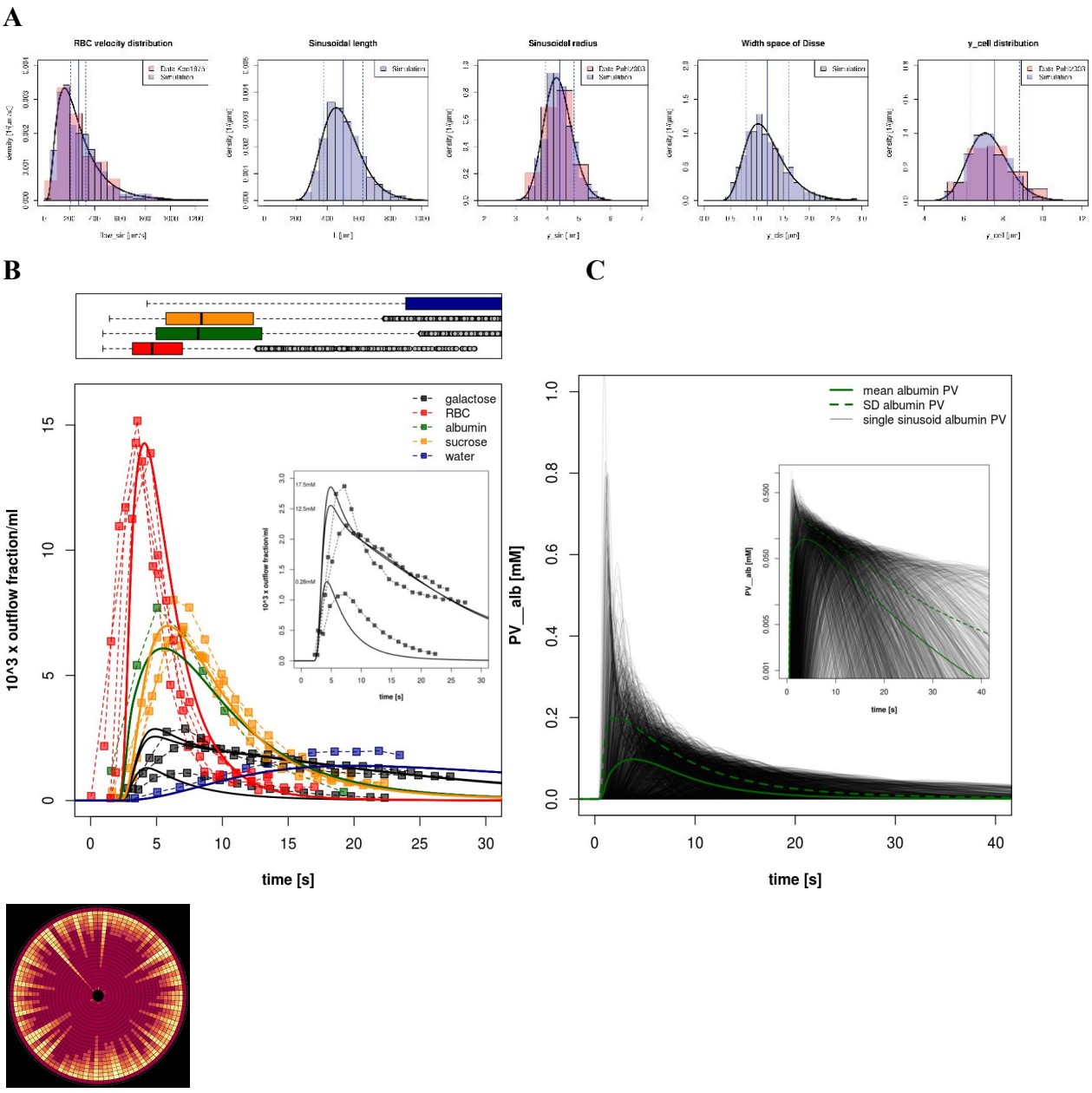

A) Experimental parameter distributions (see Supplementary Information for references) and distribution of parameter samples (N=2000) underlying calculation of multiple indicator dilution curves. To simulate the liver function of a region of interest the response of the samples of structural different sinusoidal units is integrated.

B) Resulting integrated multiple-indicator dilution curves of traced red blood cells (red), albumin (green), sucrose (orange), water (blue) and galactose (gal) after a rectangular tracer peak of duration 0.5s (see inlet) with experimental data from {Goresky1973, Goresky1983}. Three simulations corresponding to the experimental conditions of varying unlabeled galactose concentrations of 0.28mM, 12.5mM and 17.5mM are depicted. Inlet shows the multiple-indicator dilution curves of traced galactose corresponding to B. An increase in unlabeled galactose results in competitive inhibition of galactose transport into the liver.

C) Perivenous albumin concentrations of single sinusoids. Individual curves for the sampled geometries with mean (solid) and mean+-std (dashed). The response of the different sinusoids is very heterogenous and the actual dilution behavior depends strongly on the local microarchitecture.

Figure 3 *– Sinusoidal gradients in galactose metabolization*

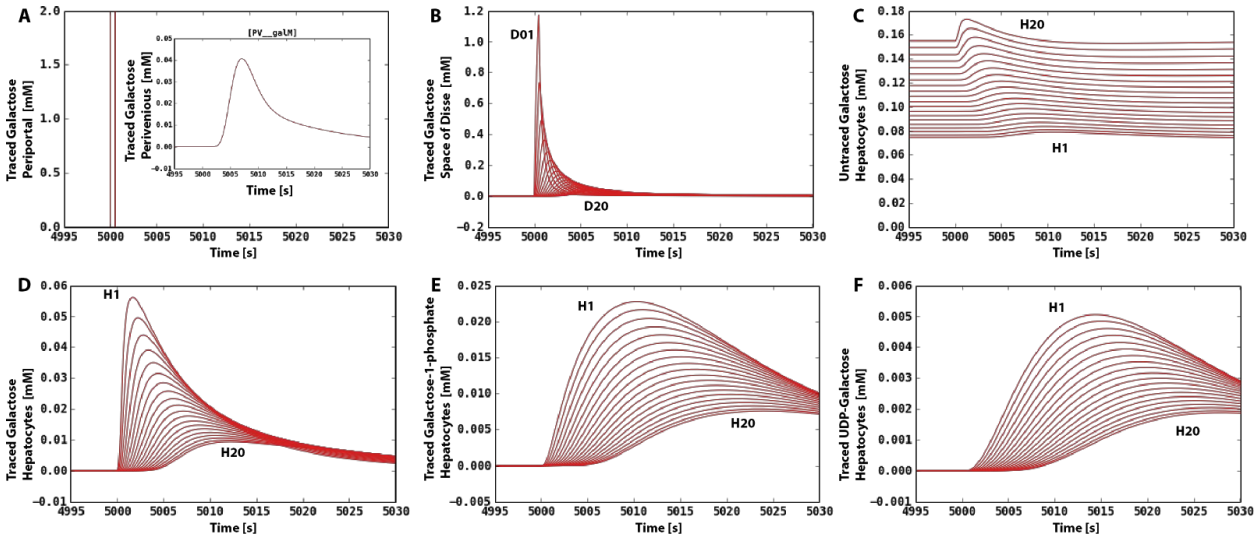

Sinusoidal gradients in galactose metabolism after traced galactose is given. Periportal traced galactose under constant untraced galactose load of 0.28mM (corresponding to lowest galactose concentration in figure 2). Simulation of a single sinusoidal unit (mean sinusoidal unit with mean structural and flow parameters) is shown.

A) Applied periportal galactose tracer (rectangular peak of duration 0.5s). Tracer is given at t=5000s after system reached steady state under the untraced galactose load. Resulting perivenous traced galactose concentration is depicted in the inlet.

B) Concentration of traced galactose in the space of Disse (Space of Disse adjacent to the first periportal hepatocyte H01 is D01, adjacent to the last perivenous hepatocyte H20 is D20.

C) Untraced galactose concentration in hepatocyte H01 (periportal) to H20 (perivenous). Untraced galactose increases in the hepatocytes along the sinusoids due to the competitive inhibition (alternative substrate) of Galactokinase via the traced galactose in the hepatocytes.

D) Traced galactose in hepatocytes along the sinusoid.

E) Traced galactose-1 phosphate in hepatocytes along the sinusoid. Galactokinase is the rate limiting step.

F) Traced UDP-galactose concentration in the hepatocytes along the sinusoid.

Figure 4 *– Hepatic galactose elimination, extraction ratio, and flow-dependent clearance and extraction ratio on tissue scale & the effect of aging (A-H) & Whole liver galactose elimination, extraction ratio, and clearance (I-O).*

A-H

I-O

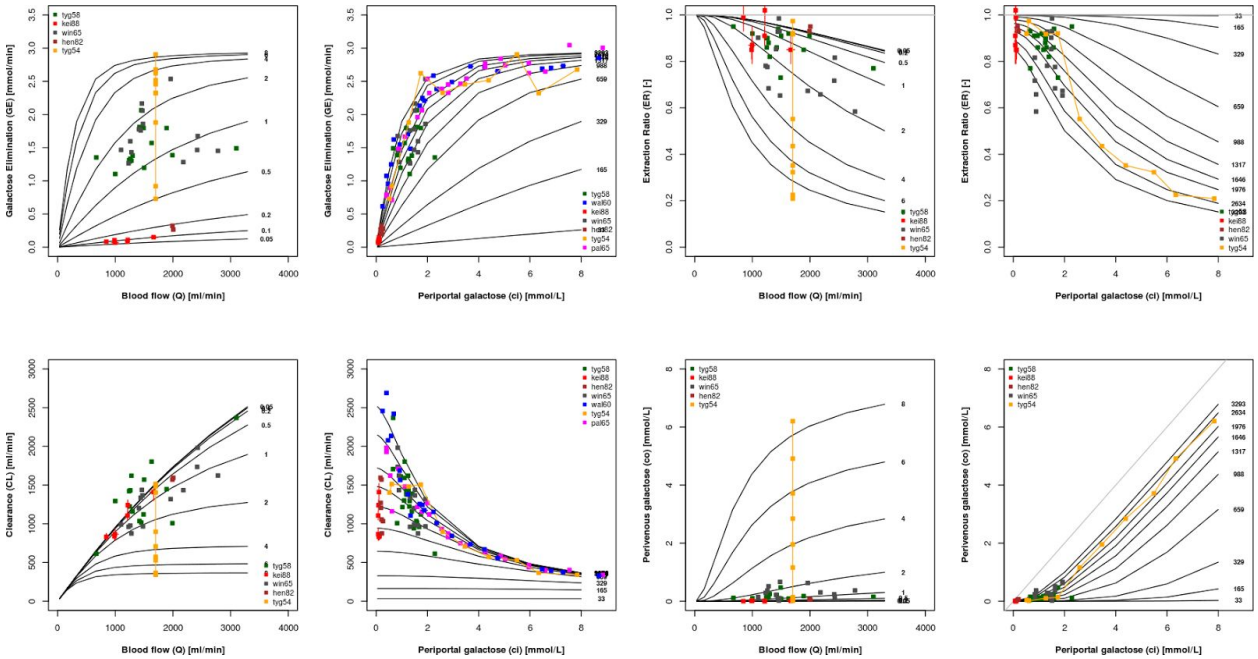

Steady state galactose elimination (GE), Clearance (CL), Extraction Ratio (ER) and perivenous galactose concentration (co) depending on blood flow and periportal galactose concentration (ci) and age dependent changes in ultrastructure (pseudocapillari

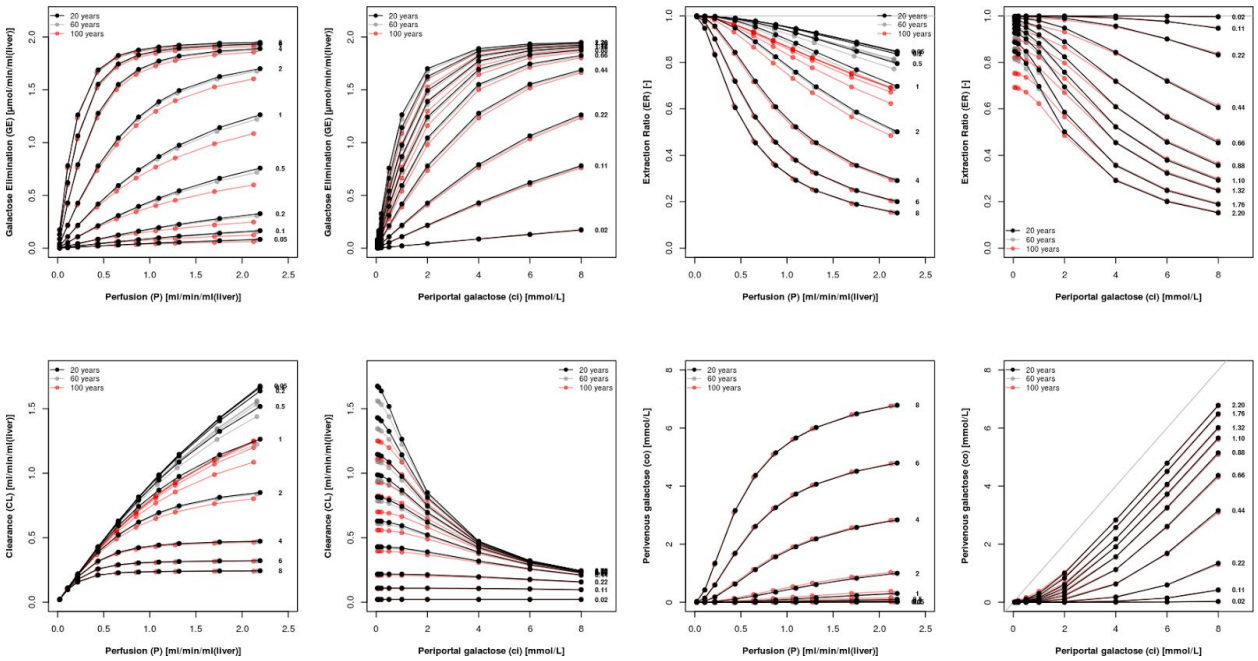

zation).

Curves for unaltered ultrastructure (corresponding to age of 20 years) in blue and advanced pseudocapillarization via defenestraetion and widening of endothelial cells (corresponding to age 100 years) in red. Every data point is the integration over N=100 simulations based on samples from the underlying ultrastructure and perfusion to steady state under the given conditions.

I-O Comparison of predictions with individual subject data in human {Keiding1988, Tygstrup1958, Tygstrup1954, Waldstein1960, Henderson1982, Winkler1965, Palu1965}

Figure 5 *– Organ heterogeneity in galactose elimination, extraction ratio, and clearance. Integration under perfusion heterogeneity of normal subjects.*

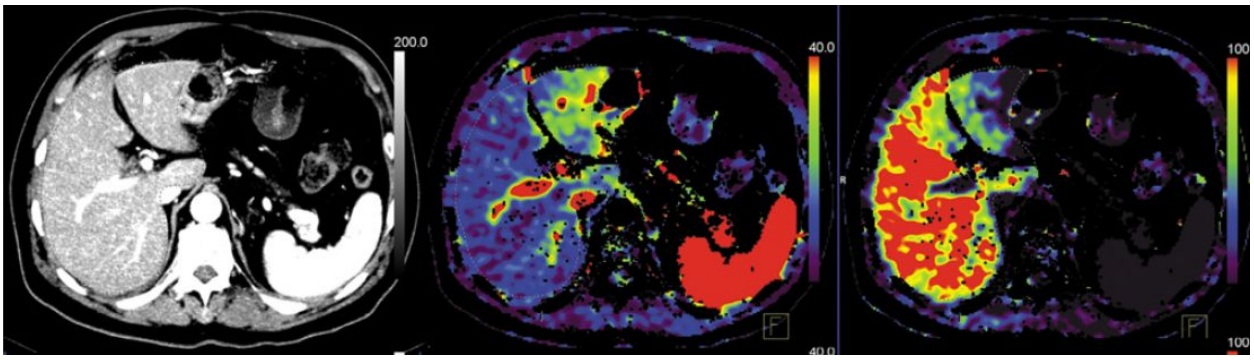

Figure 6 *– Individualized GEC prediction, prediction of population variability & age dependence and successful classification of liver disease*

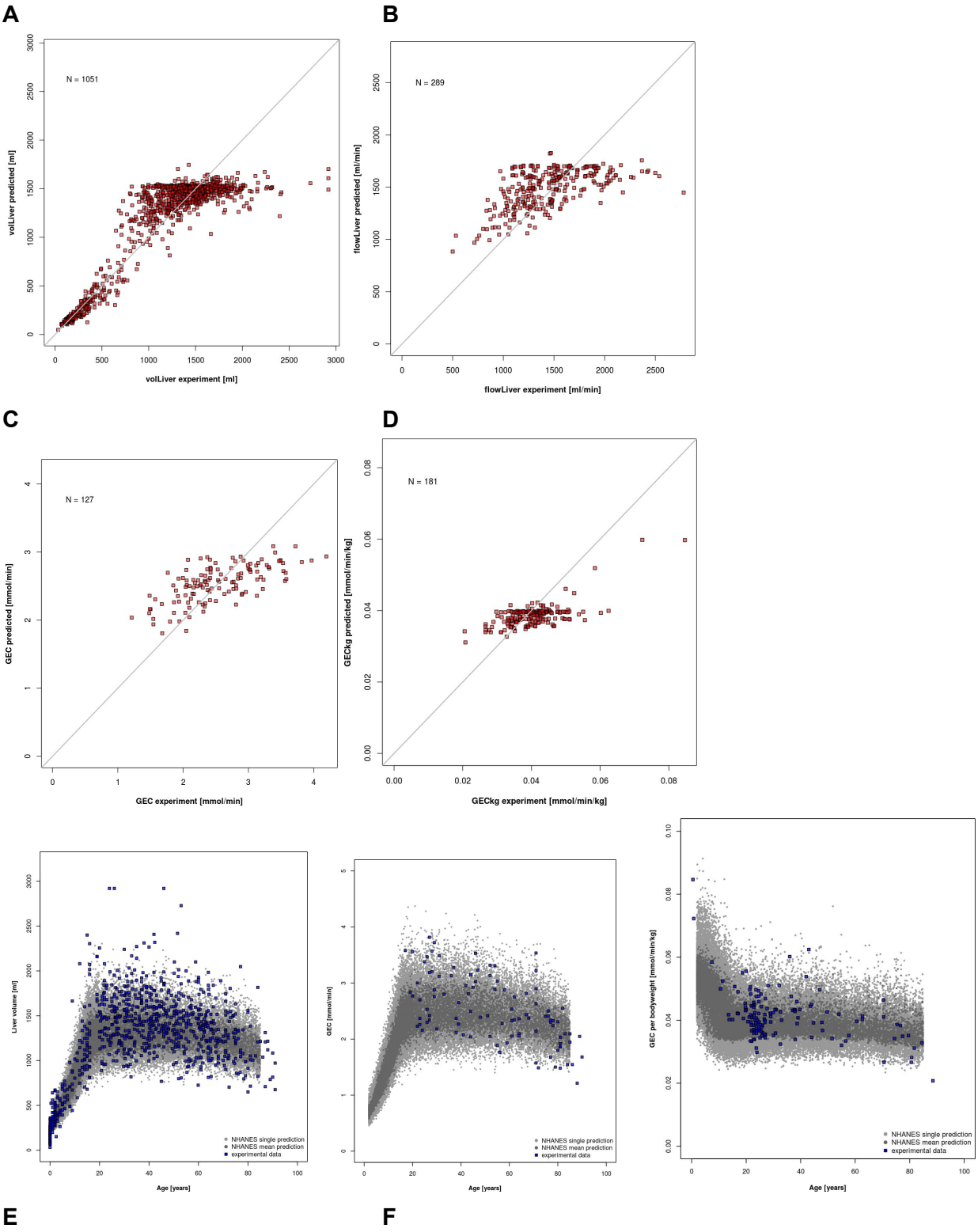

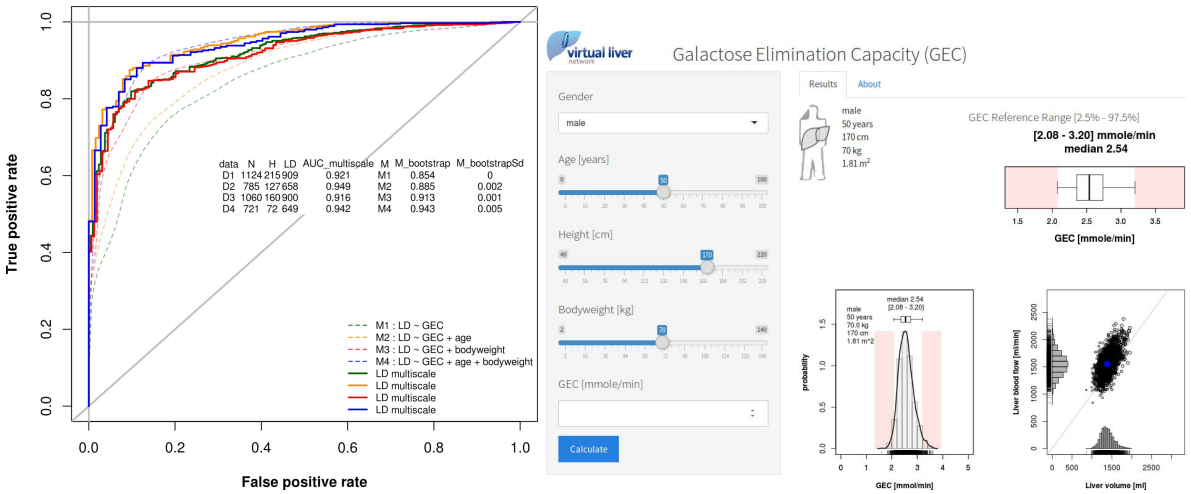

A) Prediction of normal GEC range based on the subset of available anthropomorphic information. Comparison with experimental data.
B) Prediction of normal GEC per bodyweight based on the subset of available anthropomorphic information. Comparison with experimental data (large subset of the data is independent from A, thereby providing independent validation of method.
C) Predicted population variability of GEC in healthy subjects based on the anthropomorphic infromation available in the NHANES cohort. Available experimental GEC data shown in comparison.
D) Predicted GEC per bodyweight population variability from NHANES cohort. Available experimental GEC dta shown in comparison. Large subset of GEC per bodyweight data is independent from C, providing independent validation of method.

E) Performance evaluation of individualized GEC classifier for liver disease. The multiscale classifier was compared to a series of logistic regression models using varying predictor variables. An overview about the various data subsets and the resulting areas under the curve (AUC) for the various models is given in the figure.
G) Screenshot of the web based application for prediction of GEC ranges and liver disease based on GEC measurements available at https://www.livermetabolism.com/gec_app/.